

Solving Nuclear-Structure Problems with the Adaptive Variational Quantum Algorithm

A. M. Romero*

Department of Physics and Astronomy, University of North Carolina, Chapel Hill, North Carolina 27516-3255, USA

Departament de Física Quàntica i Astrofísica (FQA),

Universitat de Barcelona (UB), c. Martí i Franqués, 1, 08028 Barcelona, Spain

Institut de Ciències del Cosmos (ICCUB), Universitat de Barcelona (UB),

c. Martí i Franqués, 1, 08028 Barcelona, Spain

J. Engel†

Department of Physics and Astronomy, University of North Carolina, Chapel Hill, North Carolina 27516-3255, USA

Ho Lun Tang‡ and Sophia E. Economou§

Department of Physics, Virginia Tech, Blacksburg, VA 24061

(Dated: June 30, 2022)

We use the Lipkin-Meshkov-Glick (LMG) model and the valence-space nuclear shell model to examine the likely performance of variational quantum eigensolvers in nuclear-structure theory. The LMG model exhibits both a phase transition and spontaneous symmetry breaking at the mean-field level in one of the phases, features that characterize collective dynamics in medium-mass and heavy nuclei. We show that with appropriate modifications, the ADAPT-VQE algorithm, a particularly flexible and accurate variational approach, is not troubled by these complications. We treat up to 12 particles and show that the number of quantum operations needed to approach the ground-state energy scales linearly with the number of qubits. We find similar scaling when the algorithm is applied to the nuclear shell model with realistic interactions in the *sd* and *pf* shells. Although most of these simulations contain no noise, we use a noise model from real IBM hardware to show that for the LMG model with four particles, weak noise has no effect on the efficiency of the algorithm.

I. INTRODUCTION

Quantum computers promise to allow quasi-exact solutions of quantum many-body problems in chemistry and physics without the exponential scaling that plagues classical methods [1]. Among the many ways of exploiting quantum computers, hybrid algorithms known as Variational Quantum Eigensolvers (VQEs) [2–5] which are based on the variational principle of quantum mechanics, are under particularly intensive development. These algorithms allocate optimization of wave functions to classical computers, using their quantum counterparts only to realize the parameterized states that the optimization scheme calls for. The result is fewer quantum operations (albeit at the expense of more measurements), leading to the hope that near-term quantum circuits, which are noisy and will be for some time to come, can implement the procedures without becoming too inaccurate. VQEs have been both tested on existing quantum processors and simulated classically for a number of simple problems in molecular chemistry [1, 6–8]. Despite the potential impact of these algorithms in nuclear structure, much less work has been done in this domain.

Computations in quantum chemistry and nuclear

structure have many similarities, but also important differences. A common approach in the two fields is the application of configuration-interaction methods in which model spaces are constructed from orbitals that can be empty or occupied. In nuclear physics such methods are generically referred to as “the shell model,” and range from the diagonalization of phenomenological nucleon-nucleon interactions in quite limited valence spaces to *ab initio* calculations with bare nucleon-nucleon interactions in many-shell model spaces with no inert “core.” The use of orbitals in nuclear physics, however, may obscure the fact that nucleons do not orbit around any fixed points. The nucleus is self bound, and the nucleons that compose it can move in concert without drastically changing their total energy. This low-energy collective motion has many consequences, the most important of which in the context of VQEs is that mean-field theory, which underlies configuration-interaction methods, must spontaneously break symmetries of the Hamiltonian — translational symmetry at least, and sometimes also rotational symmetry, parity, and particle-number conservation — to capture the collective correlations corresponding to shape deformation, superfluidity, etc. Certain symmetries are broken in some nuclei and not others, so that a quantum phase transition can occur at critical values of the neutron and/or proton number.

To assess the performance of VQEs for nuclear physics problems, we must work with relatively simple models and/or systems for which nearly exact solutions are easy to obtain. One such model, which is due to Lipkin,

* a.marquez.romero@fqa.ub.edu

† engelj@physics.unc.edu

‡ holuntang@vt.edu

§ economou@vt.edu

Meshkov, and Glick (the LMG model) [9] and which we will describe in detail in the next section, has several virtues. For certain values of its parameters, it is a simplified version of a closed-shell nucleus with an isoscalar monopole giant resonance as an excitation. When the energy of the resonance goes to zero, the model exhibits a transition to a “deformed phase” [10] very much like that associated with actual physical deformation. The symmetry that is broken in the model is “number parity,” which resembles the spatial parity broken in pear-shaped nuclei. Finally, the model can be interpreted as involving interacting spins, which has made it useful for condensed-matter physics [11–13] and for a benchmark study for quantum chemistry methods [14]. The second simple case we examine is the shell model itself, under the restriction that both the number of orbitals and the number of nucleons occupying those orbitals are reasonably small.

Two recent papers [15, 16] have examined VQEs within the LMG model. The authors of Ref. [15] focused on a small number of qubits (up to three) and used an ansatz that enforced the symmetries of the model, so as to search only the relevant subspace. Most of the analysis involved running this small version of the problem on quantum hardware and assessing the performance of the hardware when combined with error mitigation techniques. Although the symmetry-enforcing circuit was efficient in terms of gate count and number of parameters, it was limited to the (exactly solvable) LMG model. Finding an efficient state preparation circuit for larger system sizes is a nontrivial task, and Ref. [15] cited a CNOT scaling of $\mathcal{O}(2^N)$. Ref. [16] compared the unitary coupled cluster ansatz and structure-learning ansatz [17] through classical simulations of the LMG problem for up to four qubits. The performance of this ansatz declined as the interaction strength in the Hamiltonian was increased. It therefore remains an open problem to find a suitable VQE approach for the LMG model that scales favorably and that can also be generalized to realistic nuclear-structure problems (beyond solvable models) with complex physics such as phase transitions.

Studies of the quantum algorithms in the shell model are fewer. We are aware only of Ref. [18], which analyzed the efficiency of encodings and the performance of a unitary coupled clusters ansatz in four nuclei, with up to six valence nucleons.

In this paper, we address the challenge of treating the LMG model efficiently in all its complexity, and also handling the phenomenological shell model, by employing an algorithm known as Adaptive Derivative-Assembled Problem-Tailored VQE (ADAPT-VQE) [19, 20]. The ADAPT-VQE algorithm grows the ansatz iteratively and according to the Hamiltonian that is being simulated. As a result, an ansatz tailored to the problem is created through information obtained by measurements on the quantum computer. We apply ADAPT-VQE to the LMG model on both sides of the phase transition and then to the phenomenological nuclear shell model with realistic

effective interactions and relatively small numbers of particles. We investigate the scaling of circuit depth with particle number, particularly around the LMG phase transition and when the mean-field spontaneously breaks a symmetry. This is crucial to assessing the likely effectiveness of near-term quantum computers. We find extremely promising scaling in both cases, even around the phase transition, when we apply symmetry-projection techniques from nuclear-structure theory. The problem-tailored nature of the ADAPT-VQE ansatz allows the algorithm to adjust the circuit structure and depth according to the demands presented by the problem. It also enables easy implementation of additional subroutines for various purposes, such as symmetry projection. This makes ADAPT-VQE particularly well suited to problems involving a quantum phase transition, including those in nuclear physics. Our results are not only important for the quantum simulations of nuclear structure, but also serve as the first test of the ADAPT-VQE algorithm in problems that exhibit complex phenomena such as phase transitions and symmetry breaking.

The article is organized as follows. Section II introduces the LMG model and the mean-field and projection techniques that we use to construct suitable ADAPT-VQE ansatz. Section III summarizes the theory of the shell model, which we also implement in ADAPT-VQE. Section IV briefly presents the variational quantum algorithm and describes the modifications that we use to include projection. Section V presents results on the performance and scaling of the algorithms, and Sec. VI offers some conclusions.

II. LIPKIN-MESHKOV-GLICK MODEL

The LMG model [9] describes a system of N particles moving in two N -fold degenerate shells, separated from one another by a single-particle energy gap as illustrated in Fig 1. The gap mimics a similar gap between nuclear shells, so that the lowest configuration in the model represents a closed-shell nucleus.

The LMG Hamiltonian is

$$H = tJ_z - V(J_x^2 - J_y^2) = tJ_z - \frac{V}{2}(J_+^2 + J_-^2), \quad (1)$$

where J_z and $J_\pm = J_x \pm iJ_y$ are generators of an $SU(2)$ algebra obeying the commutation relations $[J_+, J_-] = 2J_z$ and $[J_z, J_\pm] = \pm J_\pm$, and are defined in terms of creation and annihilation operators for particles in the i^{th} lower ($-$) and upper ($+$) levels by the relations

$$\begin{aligned} J_z &= \frac{1}{2} \sum_i \left(a_{i,+}^\dagger a_{i,+} - a_{i,-}^\dagger a_{i,-} \right) \equiv \frac{1}{2} \sum_i \sigma_z^i, \\ J_+ &= \sum_i a_{i,+}^\dagger a_{i,-} \equiv \sum_i \sigma_+^i, \\ J_- &= \sum_i a_{i,-}^\dagger a_{i,+} \equiv \sum_i \sigma_-^i. \end{aligned} \quad (2)$$

The operator J_+ (J_-) raises (lowers) a nucleon from the lower (upper) shell to its counterpart in the upper (lower) shell, and the operator J_z is the difference between the number of nucleons in the upper and lower shell. The form of the coupling in H implies that the i^{th} lower and i^{th} upper levels must together contain a total of one nucleon, as illustrated in Fig. 1. If we take i to correspond to single-particle angular-momentum quantum numbers, it also implies that the two-nucleon part of the Hamiltonian schematically represents the piece that doesn't change a nucleon's angular momentum; it is this piece that determines the properties of monopole (breathing) resonances. Finally, as we emphasize by defining the σ operators in Eq. (2), it implies that the entire model can be taken to simulate N interacting spins, with a nucleon in the i^{th} lower (upper) level corresponding to a spinor in its down (up) state. Spins can in turn be mapped in a straightforward way to qubits.

Because the eigenstates of H are unchanged by the simultaneous scaling of t and V in Eq. (1), they really depend only a single parameter. Fixing the value of the quantity $t + (N-1)V/2$, at 1, we can, without loss of generality in the eigenvectors, write the LMG Hamiltonian in the form

$$H = \frac{1-y}{2} \sum_i \sigma_z^i - \frac{2y}{N-1} \sum_{i < j} (\sigma_+^i \sigma_+^j + \sigma_-^i \sigma_-^j), \quad (3)$$

where $y \equiv (N-1)V/2$. Varying y from 0 to 1 allows us to sample all possible values for the ratio of the two- and one-body terms in H .

The standard way to get a reasonable approximation to the ground state is through mean-field theory — the Hartree-Fock (HF) approximation in our nucleon-based interpretation. In the LMG model the HF state always has the form [10, 21]

$$\begin{aligned} |\text{HF}\rangle &= \prod_i \beta_i^\dagger |\text{vac}\rangle \\ &\equiv \prod_i [\cos(\alpha) a_{i,-}^\dagger + \sin(\alpha) a_{i,+}^\dagger] |\text{vac}\rangle, \end{aligned} \quad (4)$$

where $|\text{vac}\rangle$ is the “bare vacuum,” the state in which all the levels are unoccupied, and the β_i^\dagger create quasiparticles that are superpositions of particles in the lower and upper shells. The value of α is obtained by minimizing the expectation value of the energy in the Hartree-Fock state. One finds that α vanishes as long as the strength of the interaction, compared to the size of the single-particle splitting, is below a critical value, but becomes nonzero when the strength is above that value, viz.,

$$\cos(2\alpha) = \begin{cases} 1 & y < \frac{1}{3} \\ \frac{1-y}{2y} & y \geq \frac{1}{3}. \end{cases} \quad (5)$$

Thus, a phase transition to non-trivial quasiparticles occurs at $y = 1/3$ for any number of particles N .

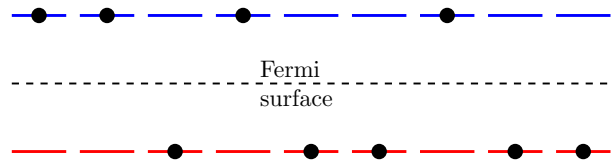


FIG. 1. One configuration of the system described by the LMG model with $N = 9$. Particles can only move directly up or down, and each pair of levels (upper and lower) must contain a total of one particle.

Instead of transforming the bare vacuum $|\text{vac}\rangle$ to the HF state $|\text{HF}\rangle$ in Eq. (4), one can retain the bare vacuum and rotate the operators in Eq. (3) around the y axis:

$$\begin{aligned} \sigma_x &\longrightarrow \cos(2\alpha)\sigma_x + \sin(2\alpha)\sigma_z, \\ \sigma_z &\longrightarrow \cos(2\alpha)\sigma_x - \sin(2\alpha)\sigma_z. \end{aligned} \quad (6)$$

The equivalence makes it easier to manipulate many-quasiparticle states.

Because the LMG Hamiltonian moves particles between the upper and lower shells only in pairs, it conserves “number parity,” the number of particles modulo 2 in the lower shell. When $y > 1/3$, however, the quasiparticle operators are superpositions of creation operators for states in both shells, and the state $|\text{HF}\rangle$ breaks number parity spontaneously [10]. The number-parity operator can be written in the form

$$\Pi \equiv (-1)^{N_+} = e^{i\pi(N/2+J_z)} = (-1)^{N/2} e^{i\pi J_z}, \quad (7)$$

and has the eigenvalue $+1$ (-1) when the system state has an even (odd) number of particles N_+ in the upper shell. Number-parity symmetry may be restored by projecting out of $|\text{HF}\rangle$ the piece with one or the other value for Π . The operator P_\pm that projects onto the space of states with even (+) or odd (−) parity is

$$P_\pm = \frac{1}{2}(1 \pm \Pi). \quad (8)$$

Like all projectors, these are Hermitian and obey $P_\pm^2 = P_\pm$.

The restoration of symmetry through projection almost always improves the accuracy of mean-field approximations in nuclear physics. Within the LMG model, the improvement can be explored both analytically [10] and, when testing approximations such as unitary coupled clusters that go beyond mean-field theory, numerically [14, 22]. Symmetry breaking and restoration has also been investigated in applications to quantum computing [23–25].

III. NUCLEAR SHELL MODEL

The shell model is a mainstay of nuclear-structure theory [26–28]. It freezes most of the nucleons in an inactive

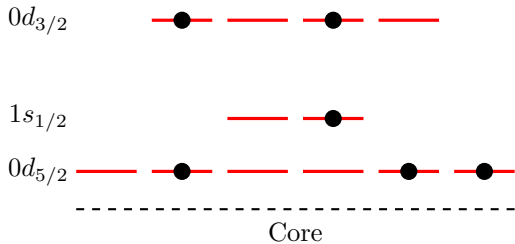


FIG. 2. One configuration of a system described by the sd -shell valence space, with $N = 6$. The orbits are degenerate and the order shown corresponds to that produced by the single-particle part of the USDB Hamiltonian.

“core,” treating only those around the Fermi surface explicitly. The various many-nucleon product states in this valence space make up a basis in which one represents a nuclear Hamiltonian. The ground and excited states of the nucleus, along with their energies, are obtained as by direct diagonalization of the Hamiltonian matrix in this effective valence space. The shell model, with a Hamiltonian derived from an underlying nucleon-nucleon interaction and then tweaked to fit the energies of particular states, is able to accurately reproduce low-lying spectra (and other properties) of many nuclei. Much like orbital-based models in chemistry, the shell model has a generic one-plus-two-body Hamiltonian, of the form

$$H = \sum_i \epsilon_i a_i^\dagger a_i + \frac{1}{4} \sum_{ijkl} \bar{v}_{ijkl} a_i^\dagger a_j^\dagger a_l a_k, \quad (9)$$

where now a_i^\dagger (a_i) creates (annihilates) a fermion in orbital i , ϵ_i is the single-particle energy of orbital i and the $\bar{v}_{ijkl} = v_{ijkl} - v_{ijlk}$ are antisymmetrized two-body matrix elements of the internucleon potential. For nuclei with mass number A between 16 and 40, one typically takes as the valence space the sd -shell, comprising the $0d_{5/2}$, $0d_{3/2}$, and $1s_{1/2}$ orbits, which amount to a total of 12 single-particle states for both protons and neutrons (a schematic of this valence space containing 6 nucleons is shown in Fig. 2). For somewhat heavier isotopes one often works in the pf -shell, comprising the $0f_{7/2}$, $0f_{5/2}$, $1p_{3/2}$, and $1p_{1/2}$ orbits and amounting to a total of 20 single-particle states for both protons and neutrons. The USDB [29] interaction is the standard two-body Hamiltonian in the sd shell, and the KB3G [30] interaction is often used in the pf shell. Ref. [18] used the sd shell in a test of the unitary coupled cluster ansatz that focused on gate depth.

IV. THE ADAPT-VQE ALGORITHM

ADAPT-VQE uses an operator pool out of which the trial state is built and a gradient criterion to determine which operator is appended at every step. The operators

are successively applied to a reference state (typically the HF state) and all the parameters are optimized at each step, starting from the previously optimized values as the initial guess. The authors of Ref. [19] simulated the use of the method on a quantum computer to calculate bond-dissociation curves for the molecules LiH, BeH₂, and H₆. The results were more accurate and required a lower circuit depth compared to those produced by other variational ansätze built from the same set of operators, such as the widely used unitary coupled cluster singles and doubles (UCCSD) [31]. ADAPT-VQE achieves shallower circuits at the cost of more measurements; considering the noisy nature of existing and near-term hardware, this trade-off is advantageous.

To analyze the performance of ADAPT-VQE in both the LMG model and the nuclear shell model, we simulate its operation on a classical computer. The quantum algorithm starts with a reference state $|\text{ref}\rangle$ and approaches the ground-state through the successive application of unitary operators, constructed by exponentiating simple excitation operators A_i from a predefined pool,

$$|n\rangle = e^{i\theta_n A_n} |n-1\rangle = \prod_{k=1}^n e^{i\theta_k A_k} |\text{ref}\rangle. \quad (10)$$

Here the θ 's are parameters with values that produce the minimum possible energy, and our convention for the product, as in Ref. [19], is $\prod_{k=1}^n \mathcal{O}_k \equiv \mathcal{O}_n \dots \mathcal{O}_1$ so that order of operators is reversed from that in the usual convention. All parameters are optimized after the application of each operator, so that $|n\rangle$ is not necessarily related simply to $|n-1\rangle$. The optimization procedure is based on the fact that the derivative of the energy at iteration n with respect to a parameter in the ansatz is the expectation value of the commutator of the corresponding pool operator with the Hamiltonian [19],

$$\frac{\partial E^{(n)}}{\partial \theta_k} = i \langle n | [H, A_k] | n \rangle. \quad (11)$$

The algorithm selects as A_{n+1} the operator that produces the largest derivative in Eq. (11); to do so it relies on the quantum circuit to construct the states in Eq. (10), from which the derivatives can be constructed by measuring the commutators. The new values for the $n+1$ parameters θ_k are then obtained by minimizing of the total energy on a classical computer with measurements of the energy on the quantum computer guiding the minimization.

To keep the circuit depth small, we restrict ourselves to a pool consisting of one- and two-body operators A_i , each of which acts on particles in at most two pairs of levels. In the LMG model, the one-body operators acting on the particles in level pair k are

$$\begin{aligned} S_+^k &= \sigma_+^k + \sigma_-^k = \sigma_x^k, \\ S_-^k &= -i(\sigma_+^k - \sigma_-^k) = \sigma_y^k, \\ S_0^k &= \sigma_z^k, \end{aligned} \quad (12)$$

where we have used the ladder Pauli operators $\sigma_{\pm} = \frac{1}{2}(\sigma_x \pm i\sigma_y)$. For the two-body operators, with $j < k$, the pool is

$$\begin{aligned}
T_+^{jk} &= \sigma_+^j \sigma_+^k + \sigma_-^j \sigma_-^k = \frac{1}{2}(\sigma_x^j \sigma_x^k - \sigma_y^j \sigma_y^k), \\
T_-^{jk} &= -i(\sigma_+^j \sigma_+^k - \sigma_-^j \sigma_-^k) = \frac{1}{2}(\sigma_x^j \sigma_y^k + \sigma_y^j \sigma_x^k), \\
U_+^{jk} &= \sigma_+^j \sigma_-^k + \sigma_-^j \sigma_+^k = \frac{1}{2}(\sigma_x^j \sigma_x^k + \sigma_y^j \sigma_y^k), \\
U_-^{jk} &= -i(\sigma_+^j \sigma_-^k - \sigma_-^j \sigma_+^k) = \frac{1}{2}(\sigma_y^j \sigma_x^k - \sigma_x^j \sigma_y^k), \\
V_+^{jk} &= (\sigma_+^j + \sigma_-^j) \sigma_z^k = \sigma_x^j \sigma_z^k, \\
V_-^{jk} &= -i(\sigma_+^j - \sigma_-^j) \sigma_z^k = \sigma_y^j \sigma_z^k, \\
V_0^{jk} &= \sigma_z^j \sigma_z^k.
\end{aligned} \tag{13}$$

The pool thus contains $3N$ one-body operators and $7N(N-1)/2$ two-body operators of each kind, exhausting all the possible Hermitian combinations of Pauli operators.

The algorithm's reference state $|\text{ref}\rangle$, the wave function at iteration zero, can be chosen freely. We use two different initial states for the LMG model: the single-configuration uncorrelated state $|0\rangle$, in which all particles are in the lower shell (or all the spins are down in the spin-model interpretation) and the mean-field Hartree-Fock state $|\text{HF}\rangle$, which spontaneously breaks number-parity symmetry for $y > 1/3$. These two states are the same for $y < 1/3$ and differ for $y > 1/3$. We can also modify the pool operators by building them from the HF quasiparticle operators β_i^\dagger and β_i in Eq. (4) rather than directly from the particle and hole operators. The use of the HF initial state and the HF quasiparticle operator pool together, is equivalent to using $|0\rangle$ and the ordinary particle-hole operator pool, with a Hamiltonian transformed according to (6).

In addition to choosing a LMG reference state, we can choose whether or not to use symmetry projection at various points in the algorithm, most easily through the ‘‘projected Hamiltonian’’ $P_+ H P_+$ (see Appendix A). To differentiate the combinations of reference states and kinds of projection that we employ in the LMG model, we use the following naming scheme for what we call ‘‘methods’’

- 0 - The reference state is the uncorrelated one, $|0\rangle$, and the operator pool contains the usual one- and two-particle-hole excitation operators.
- HF - $|\text{HF}\rangle$ is used as the initial state, together with the quasiparticle operator pool and no symmetry projection.
- HF-PAV - Same as HF except that the projected Hamiltonian $P_+ H P_+$ is monitored to assess convergence rather than H itself. The acronym PAV, which stands for ‘‘projection after variation,’’ comes from nuclear-structure theory.

- HF-VAP - Same as HF-PAV, but the projected Hamiltonian is also used to evaluate the gradients in Eq. (11) and to minimize the cost-function. This procedure is close to ‘‘variation after projection’’ in nuclear-structure theory.

ADAPT-VQE is perfectly able to handle the shell-model Hamiltonians (9) as well. Because the Hamiltonian is more general than the LMG interaction, the representation of the system in terms of qubits is more involved. Here, we will use the Jordan-Wigner mapping [32, 33] between the fermionic and Pauli operators

$$\begin{aligned}
a_i^\dagger &= \left(\prod_{k=0}^{i-1} \sigma_z^k \right) \sigma_-^i, \\
a_i &= \left(\prod_{k=0}^{i-1} \sigma_z^k \right) \sigma_+^i.
\end{aligned} \tag{14}$$

The operator pool contains all possible two-body fermion operators $a_i^\dagger a_j^\dagger a_l a_k$, where $i < j$ and $l < k$ are single-particle labels. Thus, they are of the form

$$T_{rs}^{pq} = i(a_p^\dagger a_q^\dagger a_r a_s - a_r^\dagger a_s^\dagger a_p a_q), \tag{15}$$

where antisymmetrization has been taken into account explicitly. Although shell-model Hamiltonians can break symmetries, the conserved quantities are more complicated than number-parity and we will not examine the effects of shell-model projection here.

V. RESULTS

A. LMG model

For quantum computers to be useful in the near term in nuclear physics, we need algorithms in which circuit depth increases mildly with particle number and/or model-space size. With our algorithm, this depth is related to the number of pool operators needed to approximate the exact ground state well. In Fig. 3, we plot the number of such operators (or, equivalently, the number of parameters) required to obtain the ground-state energy to within 0.1% as a function of the number of qubits N for several values of y and all the algorithm variants outlined in the previous section. For $y < 1/3$, in the symmetry-unbroken phase, the methods are all equivalent. For $y > 1/3$, the performance of different methods diverges. First, we can see that until the number of particles is sufficiently large, method HF is not as good even as method 0, particularly around the phase transition point $y = 1/3$ where the mean-field approach fails. The two symmetry-projecting methods perform the best, except for small numbers of particles, where method 0 slightly outperforms method HF-PAV. Method HF-VAP always gives the best performance. The difference between HF-VAP and HF-PAV shows that using the projected Hamiltonian for constructing the ansatz improves

the algorithm significantly. Projection in the computation of gradients is easy for ADAPT-VQE because of its flexibility; the cost-function used in the choosing operators can be modified according to the features of the problem being solved.

Once y and N are large enough, the symmetry-projecting methods do not perform substantially better than the method HF. In addition, method 0, which never breaks symmetry, does considerably worse than those that do at large y . For such “strongly deformed” systems, the crucial thing is to include important correlations in the reference state by breaking number-parity symmetry. Restoring the symmetry afterwards is less helpful; mean-field theory is all that is needed in this regime. Adding symmetry projection reduces the difficulties that mean-field theory encounters around the phase transition without affecting its performance for large y and large system size. The combination provides a universal scheme, useful for the whole range of y and N .

In Fig. 4, one can see irregularities in the curves produced by methods 0 and HF. These have to do with the criteria for convergence of the algorithm. The addition of a single operator to a chain that produces the system’s approximate state can have almost no effect or, occasionally, a large effect. If the large effect happens to reduce the energy enough so that it satisfies the convergence criterion, the iteration ends. If the effect is not quite large enough, the iteration continues and may not end until much later, when another significant reduction occurs. Fig. 5 illustrates this phenomenon. If iterations were halted when the error in the ratio of the energy to the exact one reached a little over 10^{-2} instead of 10^{-3} , the HF methods would require only about 15 operators instead of 50. In reality, of course, we don’t know the exact energy and so have to truncate when the energy appears stable. As the figure shows, and as Ref. [19] notes, long plateaus can then cause the algorithm to terminate too soon. Modifying the convergence criterion could alleviate this problem.

Figure 3 (d) and (e) show, in addition to the overall scaling already discussed, a non-monotonic trend for the HF energy as a function of the number of particles. The peak at $N = 8$ is due to a convergence plateau; at larger N , such a plateau is encountered only later, closer to the exact ground-state energy. We believe that the plateau stems from an inefficient pool or initial state (because of symmetry violation in this instance) and that the algorithm therefore needs more parameters to escape from the plateau (see the results for method HF in Fig. 5). The reason for the lower-energy plateau at larger N could be the increased efficiency of mean-field theory there.

One might expect ADAPT to be vulnerable to noise because it relies on measurements of energy gradients, which in practice are affected by imperfections in the device and controls. To address the issue of robustness against noise, we ran noisy simulations with the built-in noise model in Qiskit [34], using both real noise data from the IBM quantum device Vigo, a quantum processor

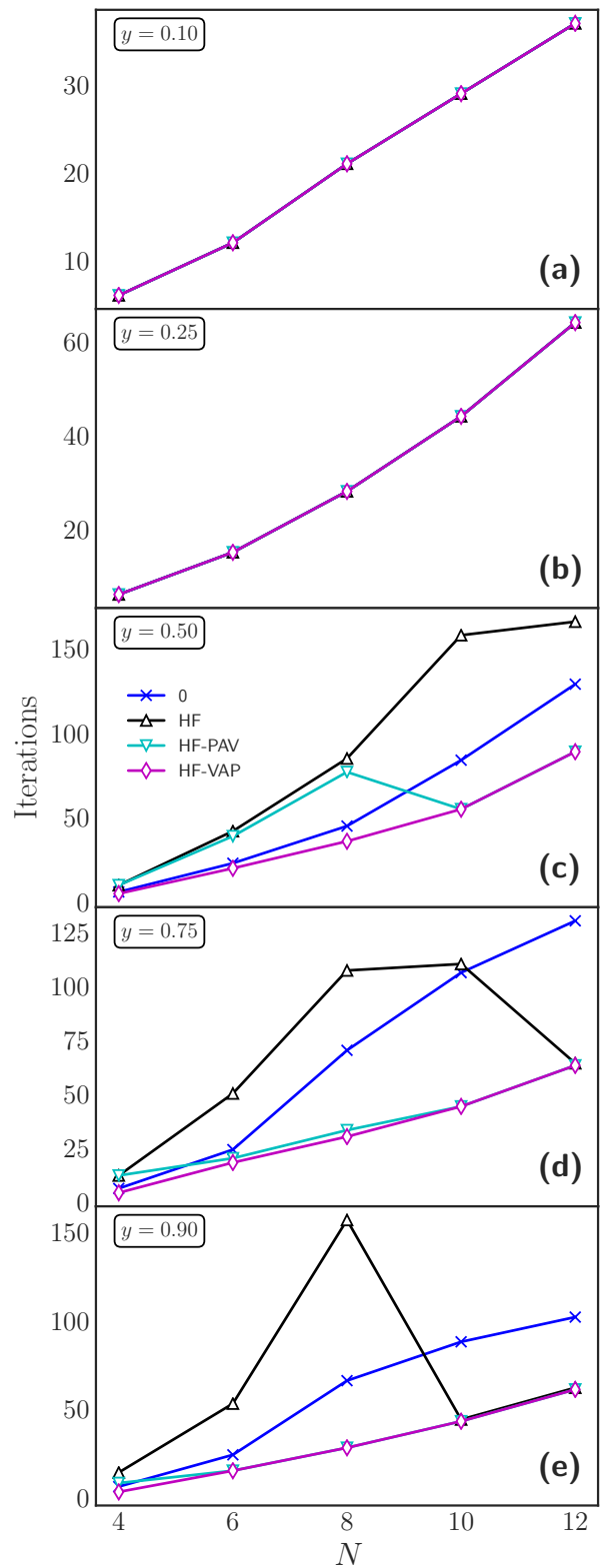


FIG. 3. Number of iterations required for ADAPT-VQE to come within 0.1% of the LMG ground-state energy, as a function of the number of particles N and for several values of the coupling constant y in the Hamiltonian (3). Each iteration corresponds to the presence of an additional pool operator in the wave function.

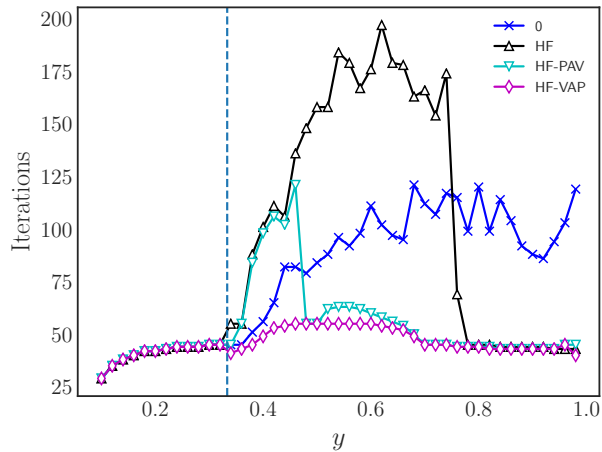


FIG. 4. Same as Fig. 3 but for a fixed number of particles ($N = 10$) and as a function of the coupling y .

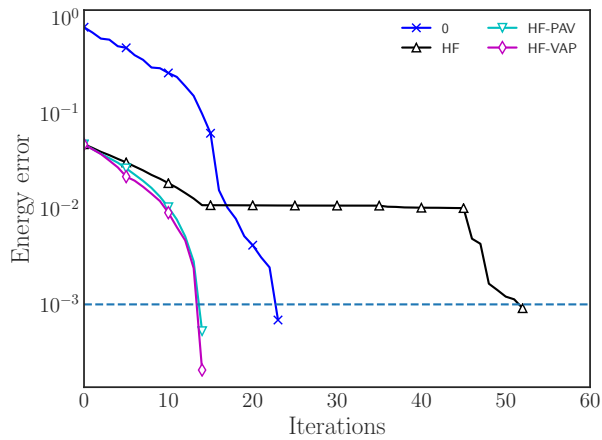


FIG. 5. Error in the ratio of the ADAPT energy to the exact one for the LMG model as a function of the number of pool operators in the ADAPT ground state, for $N = 6$ and $y = 0.9$. Method HF features a long plateau before the quick drop.

that consists of five transmons connected in a T-shaped layout, and a custom noise model. The simulation with real noise data contains gate depolarizing error, measurement error and shot noise due to finite sample size. Only gate depolarization and shot noise are included in our custom model, and we vary the gate-error rate in the model. To focus on gradient measurement, which is the distinguishing feature of ADAPT-VQE, we simulated the standard VQE part of the calculation noiselessly. The rate of convergence in the energy for the simulation with real noise and our custom model with weak noise (see Fig. 6 and its caption for details) are the same as in the noiseless simulation. This comparison shows that the algorithm is accurate as long as the noise level is below a certain threshold, i.e. that ADAPT ansatz-construction algorithm is robust. Though the effects of noise should eventually be explored in more detail, these results are

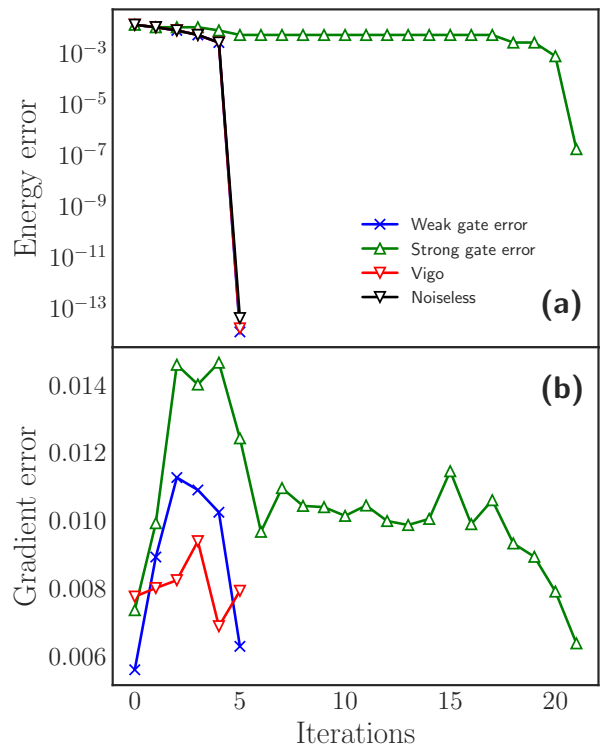


FIG. 6. Effects of noise in a simulation of ADAPT for the LMG model with $N = 4$ and $y = 0.3$, and with the uncorrelated reference state $|0\rangle$. All measurements were simulated with 8000 shots. In (a), the energy error is plotted as a function of the number of operators in the ansatz. The “weak gate error” label correspond to the custom noise model with depolarizing error rates for the single and two-qubit gates of 10% and 20%; those rates for the “strong gate error” case are 20% and 40%. The Vigo, weak noise, and noiseless results are identical. In (b), the averaged deviation of the measured derivatives from the noiseless values throughout the algorithm is plotted as a function of the number of operators in the ansatz. The errors increase with the number of iterations but only to a point, after which they decrease. The reason for the eventual decrease is that the gradient itself also eventually decrease. The “strong gate error” results show a faster increase in gradient error as the circuit grows because the gate error accumulates faster.

promising for ADAPT-VQE.

B. Nuclear shell model

In this subsection, we apply ADAPT-VQE to valence-space shell-model Hamiltonians, for isotopes in the sd and pf shells. We use the USDB and KB3G interactions mentioned in Sec. III here (with no mass-dependent modifications) together with the configuration-interaction code BIGSTICK [35, 36] whose exact results serve as a benchmark. In the sd shell, we consider isotopes of oxygen, which has no valence protons, and neon, which has two. In the pf shell we examine isotopes of calcium,

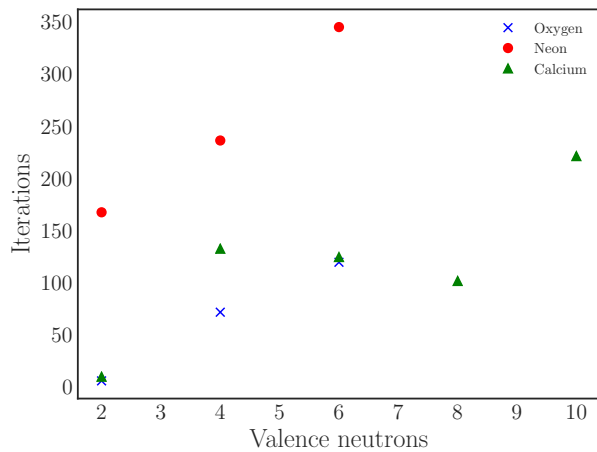


FIG. 7. Number of operators needed to reach the ground-state energy of the nucleus to within 1%, 2% and 0.0001% for isotopes of calcium, neon and oxygen, respectively, as a function of the number of valence neutrons in the shell.

which has no valence protons. Nuclei more complicated than those are a large burden for simulations. We increase the neutron number until the shell is half full; further increases reduce the dimension of the Hilbert space.

Good mean-field theory in the shell model would involve pair correlations and particle-number-violating (not number-parity-violating) reference states, and so we limit ourselves to an analog of method 0, choosing the configuration — a set of filled and empty orbitals — with the lowest average energy and choosing randomly when we encounter degeneracy. We thus violate no symmetries and need no projection. A thorough investigation of mean-field symmetry breaking in this context will be the focus of future work.

Figure 7 shows how the number of operators needed to reproduce the ground-state energies in these isotopes scales with particle number. Though the protons in neon make it more complicated than oxygen, the trend is clearly linear in both *sd*-shell isotopic chains. In calcium, a *pf*-shell chain, the sequence of points is not monotonic, for the same reasons as in the LMG model (see Fig. 3), but the rate of increase overall is low. Although we have not analyzed noise in this context, the mild scaling both here and in the LMG model is extremely promising for ADAPT-VQE.

VI. CONCLUSIONS

In this work, we have investigated the question of whether nuclear-structure physics, which encompasses collective motion, phase transitions, and complicated correlations, can potentially benefit from near-term quantum computers. By examining the scaling of the performance of ADAPT-VQE, a problem-tailored variational quantum algorithm that dynamically creates the ansatz,

in both a model-problem with many features of real nuclei and in realistic valence-space shell-model calculations, we conclude that the benefits could be substantial. We find mild scaling in all cases, including near a phase transition, if we first allow our reference state to break symmetries and then restore those symmetries before measuring energies.

The scaling we have demonstrated here, both away from the phase transition and near it, combined with a level of noise robustness in the construction of the variational ansatz, is encouraging for the future of VQEs in nuclear physics.

VII. ACKNOWLEDGMENTS

This work was supported in part by the U.S. Department of Energy Office of Science. J.E. acknowledges support from the DOE Office of Nuclear Physics, under grant No. DE-FG02-97ER41019. S.E.E. acknowledges support from the DOE National Quantum Information Science Research Centers, Co-design Center for Quantum Advantage (C2QA), contract number DE-SC0012704. Computing resources were provided by the Research Computing group at the University of North Carolina and the National Energy Research Scientific Computing Center (NERSC), a U.S. Department of Energy Office of Science User Facility located at Lawrence Berkeley National Laboratory, operated under Contract No. DE-AC02-05CH11231.

Appendix A: Computation of Projected Hamiltonian and Gradient

We write the LMG Hamiltonian in Eq. (3) in the form

$$H = \frac{1-y}{2} \sum_i \sigma_z^i - \frac{y}{N-1} \sum_{i<j} (\sigma_x^i \sigma_x^j - \sigma_y^i \sigma_y^j). \quad (\text{A1})$$

The parity projection operator is defined by Eqs. (7) and (8). Using

$$e^{i\pi J_z} = e^{i\frac{\pi}{2} \sum_j \sigma_z^j} = i^N \prod_j \sigma_z^j, \quad (\text{A2})$$

we obtain the projected Hamiltonian $P_+ H P_+ \equiv H P_+$,

$$\begin{aligned} H P_+ &= \frac{1-y}{4} \sum_i \left(\sigma_z^i + \prod_{j \neq i} \sigma_z^j \right) - \frac{1}{2} \frac{y}{N-1} \\ &\times \sum_{i<j} \left(\sigma_x^i \sigma_x^j - \sigma_y^i \sigma_y^j + \prod_{k \neq i,j} \sigma_x^k \sigma_z^i \sigma_z^j - \prod_{k \neq i,j} \sigma_y^k \sigma_z^i \sigma_z^j \right). \end{aligned} \quad (\text{A3})$$

We rotate the σ operators in this expression as in Eq. (6) to apply the VAP and PAV methods.

Method VAP requires minimizing the projected energy,

$$E_\phi = \frac{\langle \phi | HP_+ | \phi \rangle}{\langle \phi | P_+ | \phi \rangle}, \quad (\text{A4})$$

where $|\phi\rangle$ is the ansatz for the state $|n\rangle$ in Eq. (10). The supplementary information for Ref. [19] shows that without the projectors one has

$$\frac{\partial E_\phi}{\partial \theta_i} = 2 \operatorname{Re} \langle \sigma_i^H | T_i | \psi_{1,i} \rangle, \quad (\text{A5})$$

where

$$\begin{aligned} T_k &= iA_k, \\ |\sigma_i^{\mathcal{O}}\rangle &= \prod_{j=N}^{i+1} \exp(-\theta_k T_j) \mathcal{O} |\phi\rangle, \\ |\psi_{1,i}\rangle &= \prod_{j=1}^i \exp(\theta_j T_j) |0\rangle, \end{aligned} \quad (\text{A6})$$

and, as always, the usual product convention is reversed. In our case, with projectors included, this expression becomes

$$\frac{\partial E_\phi}{\partial \theta_i} = \frac{1}{|\langle \phi | P_+ | \phi \rangle|^2} \left(2 \operatorname{Re} \langle \sigma_i^{HP_+} | T_i | \psi_{1,i} \rangle \langle \phi | P_+ | \phi \rangle - 2 \operatorname{Re} \langle \sigma_i^{P_+} | T_i | \psi_{1,i} \rangle \langle \phi | HP_+ | \phi \rangle \right). \quad (\text{A7})$$

- [1] S. McArdle, S. Endo, A. Aspuru-Guzik, S. C. Benjamin, and X. Yuan, Quantum computational chemistry, *Rev. Mod. Phys.* **92**, 015003 (2020).
- [2] A. Peruzzo, J. McClean, P. Shadbolt, M.-H. Yung, X.-Q. Zhou, P. J. Love, A. Aspuru-Guzik, and J. L. O'Brien, A variational eigenvalue solver on a photonic quantum processor, *Nature communications* **5**, 1 (2014).
- [3] M. Cerezo, A. Arrasmith, R. Babbush, S. C. Benjamin, S. Endo, K. Fujii, J. R. McClean, K. Mitarai, X. Yuan, L. Cincio, and P. J. Coles, Variational quantum algorithms, *Nature Reviews Physics* **3**, 625 (2021).
- [4] J. Tilly, H. Chen, S. Cao, D. Picozzi, K. Setia, Y. Li, E. Grant, L. Wossnig, I. Rungger, G. H. Booth, and J. Tennyson, The variational quantum eigensolver: a review of methods and best practices (2021), arXiv:2111.05176 [quant-ph].
- [5] K. Bharti, A. Cervera-Lierta, T. H. Kyaw, T. Haug, S. Alperin-Lea, A. Anand, M. Degroote, H. Heimonen, J. S. Kottmann, T. Menke, *et al.*, Noisy intermediate-scale quantum (nisq) algorithms, arXiv preprint arXiv:2101.08448 (2021).
- [6] A. Kandala, A. Mezzacapo, K. Temme, M. Takita, M. Brink, J. M. Chow, and J. M. Gambetta, Hardware-efficient variational quantum eigensolver for small molecules and quantum magnets, *Nature* **549**, 242 (2017).
- [7] J. I. Colless, V. V. Ramasesh, D. Dahlen, M. S. Blok, M. E. Kimchi-Schwartz, J. R. McClean, J. Carter, W. A. de Jong, and I. Siddiqi, Computation of molecular spectra on a quantum processor with an error-resilient algorithm, *Physical Review X* **8**, 011021 (2018).
- [8] Y. Cao, J. Romero, J. P. Olson, M. Degroote, P. D. Johnson, M. Kieferová, I. D. Kivlichan, T. Menke, B. Peropadre, N. P. Sawaya, *et al.*, Quantum chemistry in the age of quantum computing, *Chemical reviews* **119**, 10856 (2019).
- [9] H. J. Lipkin, N. Meshkov, and A. Glick, Validity of many-body approximation methods for a solvable model:(i). exact solutions and perturbation theory, *Nuclear Physics* **62**, 188 (1965).
- [10] D. Agassi, H. Lipkin, and N. Meshkov, Validity of many-body approximation methods for a solvable model:(iv). the deformed hartree-fock solution, *Nuclear Physics* **86**, 321 (1966).
- [11] R. G. Unanyan, C. Ionescu, and M. Fleischhauer, Many-particle entanglement in the gaped antiferromagnetic lipkin model, *Physical Review A* **72**, 022326 (2005).
- [12] S. Campbell, Criticality revealed through quench dynamics in the lipkin-meshkov-glick model, *Physical Review B* **94**, 184403 (2016).
- [13] A. Russomanno, F. Iemini, M. Dalmonte, and R. Fazio, Floquet time crystal in the lipkin-meshkov-glick model, *Physical Review B* **95**, 214307 (2017).
- [14] J. M. Wahlen-Strothman, T. M. Henderson, M. R. Hermes, M. Degroote, Y. Qiu, J. Zhao, J. Dukelsky, and G. E. Scuseria, Merging symmetry projection methods with coupled cluster theory: Lessons from the lipkin model hamiltonian, *The Journal of chemical physics* **146**, 054110 (2017).
- [15] M. J. Cervia, A. B. Balantekin, S. N. Coppersmith, C. W. Johnson, P. J. Love, C. Poole, K. Robbins, and M. Saffman, Lipkin model on a quantum computer, *Physical Review C* **104**, 024305 (2021).
- [16] A. Chikaoka and H. Liang, Quantum computing for the lipkin model with unitary coupled cluster and structure learning ansatz, *Chinese Physics C* **46**, 024106 (2022).
- [17] M. Ostaszewski, E. Grant, and M. Benedetti, Structure optimization for parameterized quantum circuits, *Quantum* **5**, 391 (2021).
- [18] I. Stetcu, A. Baroni, and J. Carlson, Variational approaches to constructing the many-body nuclear ground state for quantum computing, arXiv preprint arXiv:2110.06098 (2021).
- [19] H. R. Grimsley, S. E. Economou, E. Barnes, and N. J. Mayhall, An adaptive variational algorithm for exact molecular simulations on a quantum computer, *Nature communications* **10**, 1 (2019).
- [20] H. L. Tang, V. O. Shkolnikov, G. S. Barron, H. R. Grimsley, N. J. Mayhall, E. Barnes, and S. E. Economou, qubit-adapt-vqe: An adaptive algorithm for construct-

- ing hardware-efficient ansätze on a quantum processor, *PRX Quantum* **2**, 020310 (2021).
- [21] P. Ring and P. Schuck, *The nuclear many-body problem* (Springer Science & Business Media, 2004).
- [22] G. Harsha, T. Shiozaki, and G. E. Scuseria, On the difference between variational and unitary coupled cluster theories, *The Journal of chemical physics* **148**, 044107 (2018).
- [23] B. T. Gard, L. Zhu, G. S. Barron, N. J. Mayhall, S. E. Economou, and E. Barnes, Efficient symmetry-preserving state preparation circuits for the variational quantum eigensolver algorithm, *npj Quantum Information* **6**, 1 (2020).
- [24] D. Lacroix, Symmetry-assisted preparation of entangled many-body states on a quantum computer, *Physical Review Letters* **125**, 230502 (2020).
- [25] E. Guzman and D. Lacroix, Accessing ground state and excited states energies in many-body system after symmetry restoration using quantum computers, arXiv preprint arXiv:2111.13080 (2021).
- [26] E. Caurier, G. Martínez-Pinedo, F. Nowacki, A. Poves, and A. P. Zuker, The shell model as a unified view of nuclear structure, *Reviews of modern Physics* **77**, 427 (2005).
- [27] K. L. Heyde, The nuclear shell model, in *The Nuclear Shell Model* (Springer, 1994) pp. 58–154.
- [28] A. De-Shalit and I. Talmi, *Nuclear shell theory*, Vol. 14 (Academic Press, 2013).
- [29] B. A. Brown and W. A. Richter, New “usd” hamiltonians for the sd shell, *Physical Review C* **74**, 034315 (2006).
- [30] A. Poves, J. Sánchez-Solano, E. Caurier, and F. Nowacki, Shell model study of the isobaric chains $a=50$, $a=51$ and $a=52$, *Nuclear Physics A* **694**, 157 (2001).
- [31] J. Lee, W. J. Huggins, M. Head-Gordon, and K. B. Whaley, Generalized unitary coupled cluster wave functions for quantum computation, *Journal of chemical theory and computation* **15**, 311 (2018).
- [32] P. Jordan and E. P. Wigner, Über das paulische äquivalenzverbot, in *The Collected Works of Eugene Paul Wigner* (Springer, 1993) pp. 109–129.
- [33] G. Ortiz, J. E. Gubernatis, E. Knill, and R. Laflamme, Quantum algorithms for fermionic simulations, *Physical Review A* **64**, 022319 (2001).
- [34] M. S. ANIS *et al.*, Qiskit: An open-source framework for quantum computing (2021).
- [35] C. W. Johnson, W. E. Ormand, K. S. McElvain, and H. Shan, Bigstick: A flexible configuration-interaction shell-model code, arXiv preprint arXiv:1801.08432 (2018).
- [36] C. W. Johnson, W. E. Ormand, and P. G. Krastev, Factorization in large-scale many-body calculations, *Computer Physics Communications* **184**, 2761 (2013).